Structural Integrity Evaluation for Interference-fit Flywheels in Reactor Coolant Pumps of Nuclear Power Plants

June-soo Park*, Ha-cheol Song, Ki-seok Yoon, Taek-sang Choi
Mechanical System Engineering Dept., Korea Power Engineering Company, Inc.,
150 Deokjin-dong, Yuseong-gu, Daejeon 305-353, Korea
Jai-hak Park
Safety Engineering Dept., College of Engineering, Chungbuk National University,
48 Gaesin-dong, Cheongju, Chungbuk 361-763, Korea

This study is concerned with structural integrity evaluations for the interference-fit flywheels in reactor coolant pumps (RCPs) of nuclear power plants. Stresses in the flywheel due to the shrinkage loads and centrifugal loads at the RCP normal operation speed, design overspeed and joint-release speed are obtained using the finite element method (FEM), where release of the deformation-controlled stresses as a result of structural interactions during rotation is considered. Fracture mechanics evaluations for a series of cracks assumed to exist in the flywheel are conducted, considering ductile (fatigue) and non-ductile fracture, and stress intensity factors are obtained for the cracks using the finite element alternating method (FEAM). From analysis results, it is found that fatigue crack growth rates calculated are negligible for smaller cracks. Meanwhile, the material resistance to non-ductile fracture in terms of the critical stress intensity factor (K_{IC}) and the nil-ductility transition reference temperature (RT_{NDT}) are governing factors for larger cracks.

Key Words : Structural Integrity, Interference-Fit, Flywheel, Residual Stress, Reactor Coolant Pum

Nomenclature

a : Inner radius of flywheel disc [mm]
b : Outer radius of flywheel disc [mm]
C_o : Scaling constant
c/a: Ratio of half length (c)-to-depth (a) of elliptical crack
da/dN : Fatigue crack growth per load cycle
E : Elastic modulus of material [KN/mm²]
K : Stress intensity factor of crack
K_I : Mode I stress intensity factor of crack
n : Slope of log (da/dN) vs. log (ΔK_I) curve
P : Primary stress intensity [N/mm²]

P_b : Primary bending stress intensity [N/mm²]
P_m : Primary membrane stress intensity [N/mm²]
Q : Secondary stress intensity [N/mm²]
R : Cyclic load ratio of K_{min} to K_{max}
r : Radial distance in flywheel disc [mm]
r_M : Mean radius of flywheel disc, (a+b)/2 [mm]
S : Scaling parameter
S_m : Design stress intensity value [N/mm²]
z : Distance in the meridional direction along the thickness of flywheel [mm]

Greek symbols

Δ : Range of cyclic stress intensity factor
θ : Angular distance in the flywheel
ν : Poisson ratio
σ_θ : Circumferential stress in the flywheel [N/mm²]

* Corresponding Author,
  E-mail : js_park@kopec.co.kr
  TEL : +82-42-868-4111; **FAX :** +82-42-863-4862
  Mechanical System Engineering Dept., Korea Power Engineering Company, Inc., 150 Deokjin-dong, Yuseong-gu, Daejeon 305-353, Korea. (Manuscript **Received** January 10, 2005; **Revised** September 15, 2005)

$\bar{\omega}$: Angular velocity [radian/s]

1. Introduction

The flywheel mounted on the motor shaft of reactor coolant pump (RCP) stores kinetic energy in order to ensure a slow decrease in coolant flow in the event of a loss of power to the pump motor. If the flywheel should fail during the plant normal operation, high-energy missiles and excessive vibration of the RCP assembly is generated. Also, pump rotor overspeeds to be attained during plant transients or loss-of-coolant-accidents (LOCA) increase kinetic energy of the flywheel and potential for its failure. Regulatory guidelines of the material and fabrication, design evaluation, test and inspection of the RCP flywheels apply (USNRC Reg.1.14, 1975; ASME BPVC SECTION II, 2001; ASME BPVC SECTION III, 2001; ASME BPVC SECTION XI, 2001). Critical velocities for ductile or non-ductile fracture and excessive deformation, which are applied to the flywheels with keys or splines, may not be applied to the flywheels that utilize interference-fit only (without keys or splines). Incidents of cracking of the RCP flywheel have rarely been occurred, but nevertheless the structural integrity of the RCP flywheel is safety significance due to the potential consequences from missile damage to safety-related systems (USNRC Reg.1.14, 1975; USNRC Information Notice No. 84-92, 1984; Riccardella et al., 1974).

For interference-fit flywheels, there are two types of load to be considered, i.e., the shrinkage load due to interference fitting and the centrifugal load due to rotation. Any loads to be experienced in the events of earthquakes or pipe breaks are considered for the shaft and bearings supporting the flywheel assembly. Stresses caused by shrinkage loads are deformation-controlled in nature, while those by centrifugal loads are load-controlled. Stress analysis and structural integrity evaluation for the interference-fit flywheel assembly should appropriately consider such loads and associated structural interactions during rotation. Traditionally, the thin-shell theory has been utilized in the stress analysis of the interference-fit

flywheel and, in the subsequent structural integrity evaluation, effects of release or redistribution of the secondary (interference-fit) stresses due to crack growths have been neglected (Riccardella et al., 1974).

The purpose of this study is to develop the design evaluation methodology for interference-fit flywheels and associated analysis procedures using the finite element method (FEM) model for stress analysis together with the finite element alternating method for the subsequent structural integrity evaluation. The work performed in this study covers numerical analyses of stress and deformation in the flywheel assembly using the FEM, and the linear elastic fracture mechanics (LEFM) evaluation for non-ductile or ductile fracture using the FEAM. The FEAM is used to calculate LEFM parameters (K_I) of crack in the field of residual (interference) and operational (centrifugal) stresses. Compared with the conventional methods utilized elsewhere (Bae et al., 2002; Song et al., 2002), advantages that can be obtained by applying the FEM and FEAM are discussed in the following sections.

2. Stress Analysis of Flywheel Assembly

2.1 Stress analysis model

The interference-fit flywheel being investigated here consists of a disc and a cone-shaped intermediate bushing, which are assembled by means of an interference-fit and then are shrunk onto the motor shaft. The material used for both the flywheel disc and bushing is a ductile forging of 26 NiCrMoV 14.5 (German Standard), similar to SA-508 Class 2 of American Society of Mechanical Engineers (ASME) Code (ASME BPVC SECTION II, 2001). The material for motor shaft is a low alloy (ferritic) steel forging similar to SA-182 Grade F6NM (13Cr4Ni). The initial interference or shrinkage dimensions in the radial direction are set to 0.39 mm between the flywheel disc and intermediate bushing and to 0.238 mm between the intermediate bushing and motor shaft. This interference values account for effects of the surface roughness of materials involved and
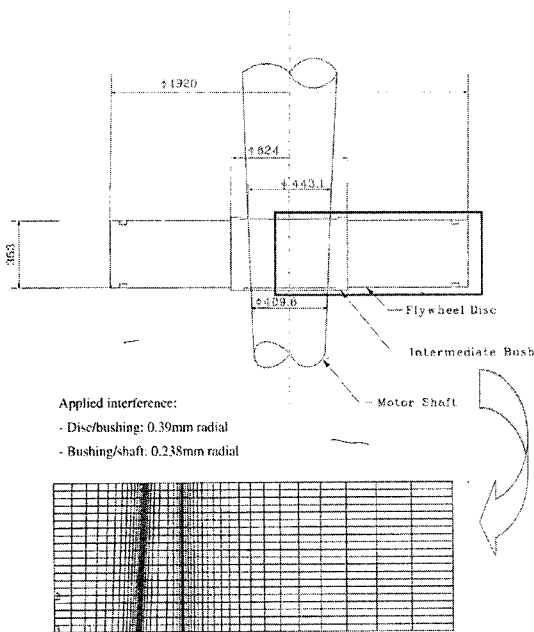
Fig. 1 Physical configuration of interference-fit fly-
wheel assembly for reactor coolant pump
(Top) and FEA model for the flywheel as-
sembly (Bottom)

of the displacements generated in the flywheel
assembly during the shaft rotation. Physical con-
figuration of the flywheel assembly with dimen-
sions in mm is shown in Fig. 1, together with the
axisymmetric finite element model used for stress
analyses. Although not shown in this figure, a set
of retention rings are provided on the shaft to
retain the flywheel disc and bushing when ap-
proaching the joint release speed of rotation.

Considering structural loads due to both the
interference-fit and the centrifugal loads generat-
ed by the rotation, stresses in the interference-fit
flywheel assembly are solved by the FEM model.
The general purpose FEM program ABAQUS/
Standard (Hibbit, Karlsson & Sorensen, Inc.,
1998) is used for stress analyses. A total of 1042
first-order isoparametric elements (CAX4) are
used for the axisymmetric model exploiting ap-
propriate boundary conditions. To resolve the
interference applied in the flywheel assembly, fit-
ting surfaces and associated contact pairs are
defined using the master and slave surface options
provided in ABAQUS : Motor shaft-to-interme-

diate bushing contact in the finite sliding condi-
tion and intermediate bushing-to-flywheel disc
in the small sliding condition. Considering ma-
terials behavior under the given interference
loads, the elastic analysis is required. Material
constants applied to the bushing and flywheel
disc are the Young's modulus (E=204 KN/mm^2)
and Poisson ratio (ν=0.3), while the shaft mate-
rial is assumed rigid.

The FEM stress solutions proceed in three
steps simulating step-by-step the interference and
operational loads. The first step is to assemble
the intermediate bushing and flywheel disc: In
this step, the static analysis option 'CONTACT
INTERFERENCE' is used to resolve the given
initial interference, while FE meshes for the mo-
tor shaft are removed from the solution domain.
The second step is to assemble the motor shaft
and the intermediate bushing and flywheel disc
already assembled together in the previous step :
The FE meshes of motor shaft previously re-
moved are restored and the given initial inter-
ference between the bushing and shaft is now
resolved. In these steps top surfaces of the shaft,
bushing, and flywheel disc are constrained in
the meridional (thickness) direction of flywheel
disc. The final step is to apply centrifugal loads
due to rotational speeds of as-shrunk flywheel
assembly. Speeds of rotation considered are the
normal operation speed, design overspeed, and
joint-release speed. During the last step, effects of
deformation in the flywheel assembly on the de-
formation-controlled stresses are taken into ac-
count. The resultant stresses in the flywheel as-
sembly, after the second step is complete, are
residual stresses at standstill. While, after the final
step, the resulting shrinkage stress (due to radial
deformation) and the centrifugal stress to rota-
tion are obtained.

2.2 Results of stress analysis

Results of FE stress analyses and non-ductile
and ductile failure assessments of the interfer-
ence-fit flywheel assembly are obtained for the
given conditions of initial interference and for
rotation speeds of the motor shaft : the standstill,
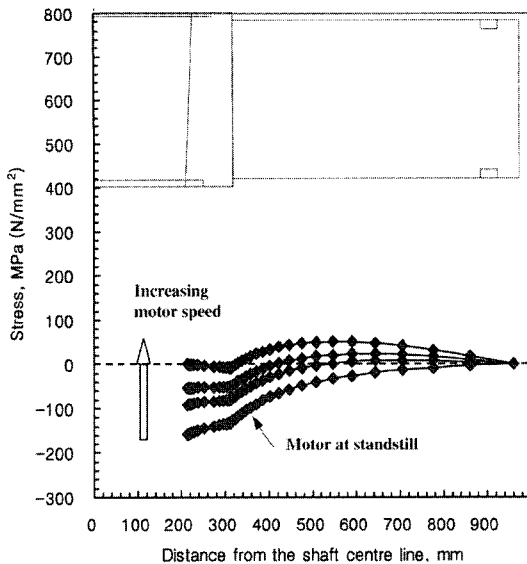normal operation, design overspeed, and joint-

Fig. 2 Variations of radial stresses (i.e., Contact Pressure) in the intermediate bushing and flywheel disc at standstill and rotating speeds of 1200, 1500, and 1875 rpm

Fig. 3 Variations of circumferential stresses in the intermediate bushing and flywheel disc at standstill and rotating speeds of 1200, 1500, and 1875 rpm

release speed. Radial stresses in the flywheel disc and intermediate bushing are shown in Fig. 2, as a function of flywheel velocity and distance from the shaft centerline. Radial stresses at both sides of the intermediate bushing acting as the contact pressure are found to remain compressive as the rotation speed varies from the standstill up to a joint-release speed of 1875 rpm. At the joint-release speed, the assembly joint of the intermediate bushing and flywheel disc is released by losing the contact pressure acting on them. This is caused by radial displacements in the flywheel at the joint-release speed of rotation. The circumferential stresses developed at various locations in the flywheel assembly are plotted in Fig. 3. The circumferential stresses in the intermediate bushing are found to be compressive under the angular velocities considered but those of the flywheel disc decrease as a function of angular velocity as the stress peak crossed the bushing-to-disc interface. The radial and circumferential stresses developed in the bushing and flywheel disc are found to increase as a function of angular velocity. However, the Mises equivalent stresses on the surface of the center bore of the flywheel
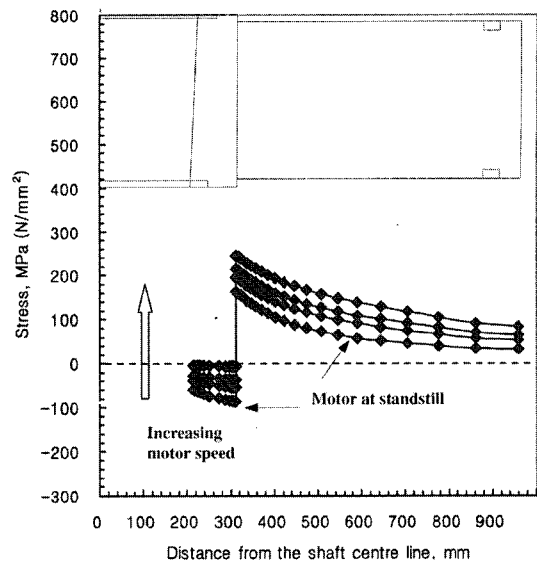
disc, though not presented here, remain at a level of about $250 \, \text{N/mm}^2$ regardless of the speed of rotation.

2.3 Stress evaluation by design analogy

Evaluations of the structural integrity for flywheel assembly require stresses in the structure be categorized into primary and secondary stresses considering different failure mechanisms. Interference loads during the thermal assembly cause the secondary stresses, while centrifugal loads during the flywheel rotation produce the primary stresses and also relax the initial interference loads. Following the design analogy of the ASME Code design rules, the primary stresses in the flywheel are determined and can be further categorized into the primary membrane (P_m) and bending stresses (P_b) by the linearization rules using the following equations (Riccardella et al., 1974).

$$P_m = \frac{1}{b-a} \int_a^b \sigma_\theta(r) \, dr \qquad (1)$$

$$P_b = \frac{6}{(b-a)^2} \int_a^b (r_M - r) \, \sigma_\theta(r) \, dr \qquad (2)$$

In these equations above, a is the inner radius

Table 1 Summary of flywheel stress analyses

Service conditions	Stress category	Stress intensity (N/mm²)	Remark
Normal	P_m	37.9	$S_m = 207$ N/mm² (30 ksi)
	P_b	44.7	
	Q	99.7	
	$P + Q$	182.3	
Faulted	P_m	75.5	
	P_b	51.8	
	Q	64.3	
	$P + Q$	191.6	

of flywheel disk, b the outer radius of flywheel disc, r_M the mean radius of flywheel disc, r the radial distance in flywheel disc, and σ_θ the circumferential stress in the flywheel. Considering characteristics of the stresses produced in the flywheel assembly, axial stresses in the flywheel may be considered insignificant and the radial stress always falls between the axial direction stress and the circumferential stress for all loading conditions. Then the maximum stress intensity at any point in the flywheel is equal to the circumferential stress. Results of the stress analyses of the flywheel are summarized in Table 1, where Normal Condition corresponds to Level A Service Condition, and Faulted Condition to Level D Service Condition (ASME BPVC SECTION III, 2001). The total stresses $(P+Q)$ in the flywheel at the normal operation (Service Level A) and at the design overspeed (Service Level D) are found as 0.88 S_m and 0.925 S_m, respectively, where P stands for the primary stress intensity and Q the secondary stress intensity.

3. Fracture Mechanics Evaluation for Flywheel

3.1 The FEAM fracture mechanics analysis model

Using results of stress analyses described in the previous section, non-ductile and ductile fracture evaluations for the interference-fit flywheel assembly are performed. A series of surface defects or cracks are assumed to exist in the flywheel disc and the mode-I stress intensity factors (K_I) are calculated based on the LEFM principles. For the fracture analysis, an analogy to the design of nuclear pressure vessels is considered and the method and procedures employed are in accordance with the rules of Appendix G of the ASME Code Section III (ASME BPVC SECTION III, 2001). A sharp, radial full-depth crack emanating from the bore at the center of the rotating flywheel disc is postulated. For the fatigue evaluation, i.e., fatigue cracks are assumed to exist inside the surface of the bore and their growth rates are evaluated. A series of semi-elliptical surface cracks are assumed to be present on the wall of the center bore in the flywheel disc, for which the circumferential component of stresses in the flywheel plays major roles in the crack growth. Similarly, a series of quarter-elliptical surface cracks are also assumed to exist at the corner (top edge) in the center bore. Stress intensity factors along the crack front are calculated, and the fatigue crack growth rate obtained by substituting the value of K into a proper crack growth equation.

A flow chart for calculating the stress intensity factors for cracks by the FEAM is given in Fig. 4. Using the FEAM, values of K are determined applying the residual shrinkage (interference-fit) stress field and the centrifugal stress field, respectively. In the FEAM, the solution of a finite body with a crack is obtained as a superposition of two solutions; an FEM solution for the finite body without a crack and an analytical solution for an infinite body with a crack. Let the circumferential component of the stress be $\sigma_\theta(r, z)$ on the $\theta = 0$ plane in the flywheel disc without a crack. Then the mode I stress intensity factor (K_I) of a meridional crack lying on the $\theta = 0$ plane can be obtained as $-\sigma_\theta(r, z)$ which is applied on the upper and lower crack surfaces as external loads. Detail descriptions on the method and numerical verification on the accuracy are given elsewhere (Nikishkov et al., 2001; Park et al., 2004; Kamaya et al., 2004).

Since a crack is not included in the three-dimensional finite element model, it is easy to
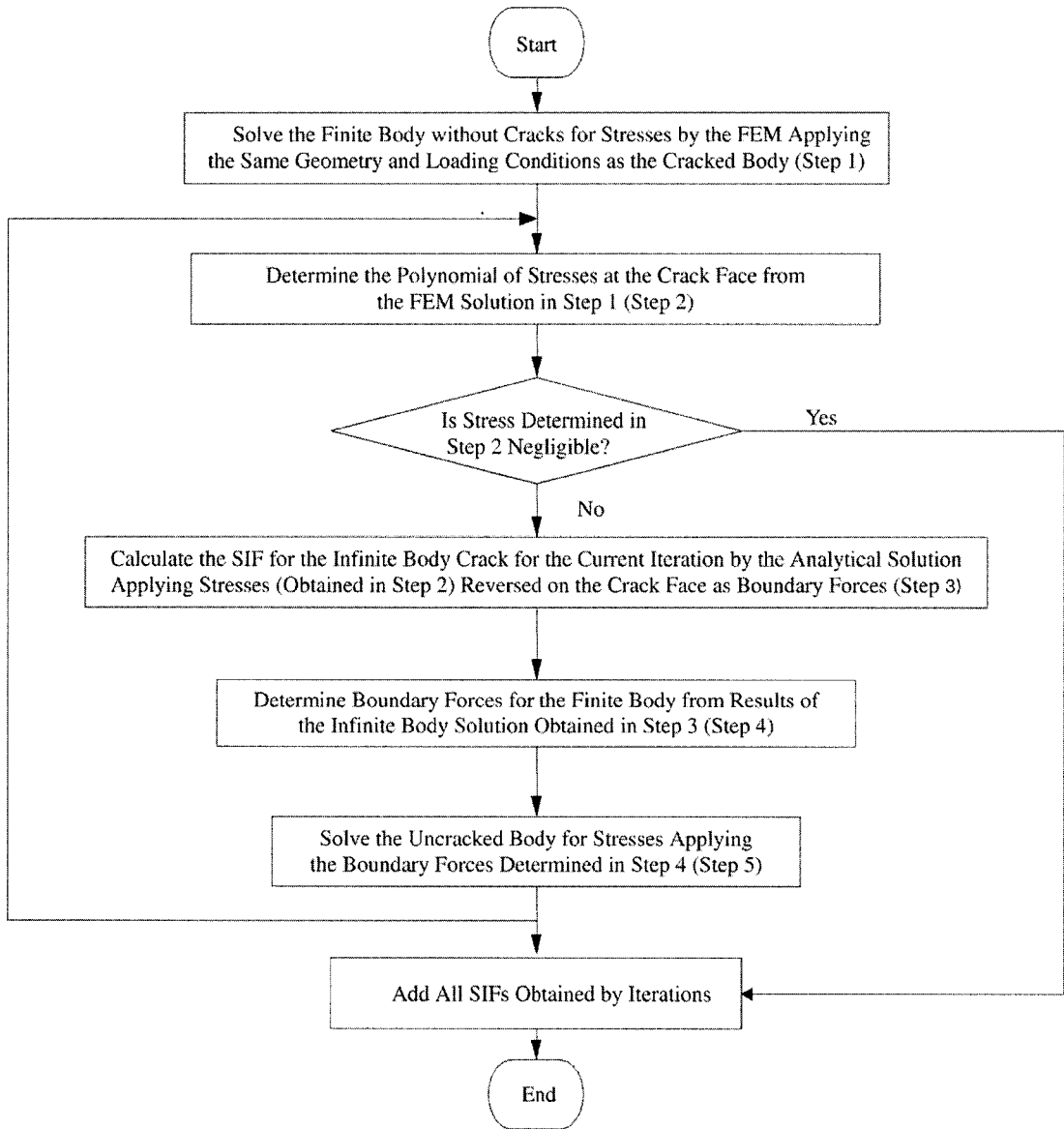
```
                              ┌──────────┐
                              │  Start   │
                              └────┬─────┘
                                   ▼
  ┌──────────────────────────────────────────────────────────────────┐
  │  Solve the Finite Body without Cracks for Stresses by the FEM      │
  │  Applying the Same Geometry and Loading Conditions as the          │
  │  Cracked Body (Step 1)                                             │
  └──────────────────────────────────┬───────────────────────────────┘
                                      ▼
        ┌──────────────────────────────────────────────────────┐
        │  Determine the Polynomial of Stresses at the Crack     │
        │  Face from the FEM Solution in Step 1 (Step 2)         │
        └──────────────────────────┬───────────────────────────┘
                                   ▼
               ◇ Is Stress Determined in Step 2 Negligible? ◇ ── Yes ──┐
                                   │                                    │
                                  No                                    │
                                   ▼                                    │
  ┌──────────────────────────────────────────────────────────────────┐│
  │  Calculate the SIF for the Infinite Body Crack for the Current     ││
  │  Iteration by the Analytical Solution Applying Stresses (Obtained  ││
  │  in Step 2) Reversed on the Crack Face as Boundary Forces (Step 3) ││
  └──────────────────────────────────┬───────────────────────────────┘│
                                      ▼                                 │
        ┌──────────────────────────────────────────────────────┐      │
        │  Determine Boundary Forces for the Finite Body from    │      │
        │  Results of the Infinite Body Solution Obtained in     │      │
        │  Step 3 (Step 4)                                       │      │
        └──────────────────────────┬───────────────────────────┘      │
                                   ▼                                    │
        ┌──────────────────────────────────────────────────────┐      │
        │  Solve the Uncracked Body for Stresses Applying the    │      │
        │  Boundary Forces Determined in Step 4 (Step 5)         │      │
        └──────────────────────────┬───────────────────────────┘      │
                                   ▼                                    │
  ┌──────────────────────────────────────────────────────┐ ◄──────────┘
  │  Add All SIFs Obtained by Iterations                   │
  └──────────────────────────┬───────────────────────────┘
                             ▼
                        ┌─────────┐
                        │   End   │
                        └─────────┘
```

Fig. 4 Flow chart for calculating stress intensity factors for cracks by the finite element alternating method

prepare the model. And the remesh procedure is not necessary in the crack growth analysis. In the analytical solution of FEAM, a crack is modeled as a continuous distribution of displacement discontinuities and an integral equation is formulated and solved by using the symmetric Galerkin method. A semi-elliptical surface crack is defined in Fig. 5 : The 'a' represents the crack depth on inner wall surface of the center bore of the flywheel disc and the '$2c$' is the crack length. In this

analysis aspect ratio of $2c/a=5$ is assumed for the crack. In the FEAM solution domain, the crack is divided into a number of crack elements. When an 8-noded element is used as a crack element, the stress singularity at the crack front can be expressed by shifting the mid-side nodes towards the crack front by one quarter of the side length of the crack element. As shown in Fig. 5, the crack mesh for a full elliptical crack is used in the analysis of a semi-elliptical crack. So the
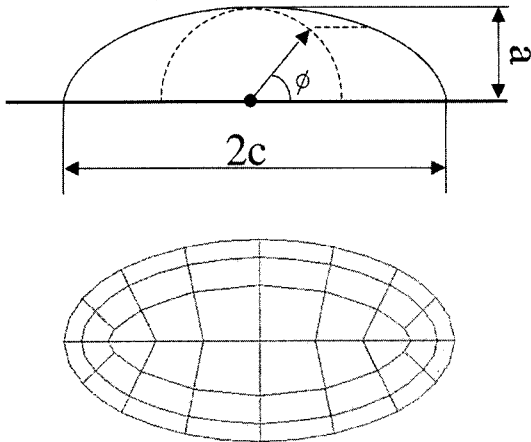
Fig. 5 Definition of crack to be used in the finite element alternating method
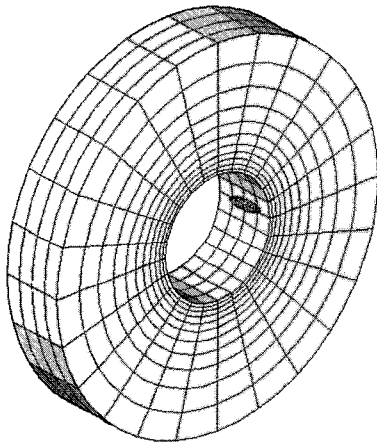

Fig. 6 The FEAM solution domain of the flywheel disc with the surface crack inside the center bore

half of the mesh corresponds to the real crack and the other half corresponds to the fictitious one. It has been known that adding of the fictitious crack mesh increases the accuracy in the FEAM (Nikishkov et al., 2001). The values of K_I are calculated from the displacement discontinuity values between the upper and lower crack surfaces near the crack front. The FEAM model for fracture mechanics analyses are defined from the 3D FEM model: See the 3D FEAM solution domain in Fig. 6, consisting of 8-noded brick-type elements of the flywheel disc and surface crack. The K_I distributions are obtained for the

semi-elliptical or quarter-elliptical cracks. The model is assumed to have the elastic constants of $E=204$ KN/mm² and $\nu=0.3$.

3.2 Calculation of fatigue crack growths

Fatigue crack growth rates are calculated by the formula in Eq. (3).

$$\frac{da}{dN}=C_o(\Delta K_I)^n \qquad (3)$$

In the equation above, da/dN is the crack growth rate (in/cycle), n is the slope of log (da/dN) versus log (ΔK_I), and C_0 the scaling constant. The crack growth rate is affected by the R ratio $(K_{\min}/K_{\max})$, where $0 \le R < 1.0$ and the environment. The reference crack growth rate for carbon and low alloy steels exposed to an atmosphere is provided with the parameters $n=3.07$ and $C_0=1.99 \times 10^{-10} S$, where S is a scaling parameter to account for the R ratio and is given by $S=25.72 \times (2.88-R)^{-3.07}$. Since the maximum stress intensity range occurs between RCP shutdown (standstill) and the normal operation speed of 1200 rpm, the R ratio is 0.785, and $S=2.656$. For the flywheel material, fatigue crack growth rates can be estimated using the following equation.

$$\frac{da}{dN}=7.06 \times 10^{-12}(\Delta K_I)^{3.07} \qquad (4)$$

Where, da/dN is m/cycle and ΔK_I in MPa m$^{1/2}$.

3.3 Results of structural integrity evaluation

For structural integrity evaluations of ductile or non-ductile fracture for the flywheel assembly, each five cases of postulated semi- and quarter-elliptical cracks are considered. Semi-elliptical surface cracks are meridionally located inside the center bore of the flywheel disc, with their maximum depths at the mid-point of the thickness and the quarter-elliptical cracks are located at the edge of the flywheel disc, with their maximum depths at the top-point of the thickness. Depths of crack considered are 2.5, 5, 10, 20, and 40 mm with the aspect ratio of crack $2c/a=5$. The crack depth of 76 mm corresponds to a through-thickness infinite crack considered to be a non-ductile fracture analysis in accordance with

the requirements of Appendix G, Section III of the ASME Code (ASME BPVC SECTION III, 2001). For all cases, the circumferential stresses in the flywheel caused by the interference-fit (shrinkage) and centrifugal loads are considered as the major crack driving forces. Stress intensity factors (K_I) of postulated cracks calculated by the FEAM are presented in Figs. 7 to 9. The dark spot in each FE model contained in these figures indicates the surface crack considered. Calculated growth rates of the cracks by fatigue are shown in Fig. 10, which are based on the ranges of K_I between the standstill and normal operation condition for the flywheel.

Figure 7 shows the K_I values determined for the semi-elliptical surface cracks in the bore of the flywheel disc at the normal operation speed. In this figure, the total value is the sum of K_I contributed by the shrinkage and centrifugal stresses and as shown for comparisons the dotted line corresponds to K_I values caused by the interference-fit for the standstill flywheel. It is noted that the crack driving force due to the centrifugal loads increases monotonically as the crack depth increases, while the one due to the shrinkage stresses increases in the range of smaller depths but saturates for larger depths. As the crack depth

increases the total K_I at the rotation speed of normal operation is significantly deviated from that of standstill, which is a combined result of the increased centrifugal stresses by rotation and of the reduced shrinkage stresses by radial deformation.

The K_I values are determined for quarter-elliptical cracks located at the edge of the center bore of the flywheel disc at normal speed and are presented in Fig. 8. The total value is the sum of K_I contributed by the shrinkage and centrifugal stresses, and the dotted line corresponds to K_I values caused by the interference-fit for the standstill flywheel. The crack driving force caused by the centrifugal and shrinkage loads is increased monotonically as the crack depth increases. Also, the total value of K_I deviates from that of standstill as the depth increases.

Stress intensity factors (K_I) for the semi-elliptical surface cracks with a depth of $a=40$ mm and located inside the center bore of the flywheel disc are plotted in Fig. 9, as a function of angular velocity of the flywheel. The resulted total K_I value of the crack is 44.2 MPa m$^{1/2}$ at the standstill caused solely by shrinkage stresses, while it increases to a value of 70.5 MPa m$^{1/2}$ at the joint-release speed. It is shown in Fig. 9 that
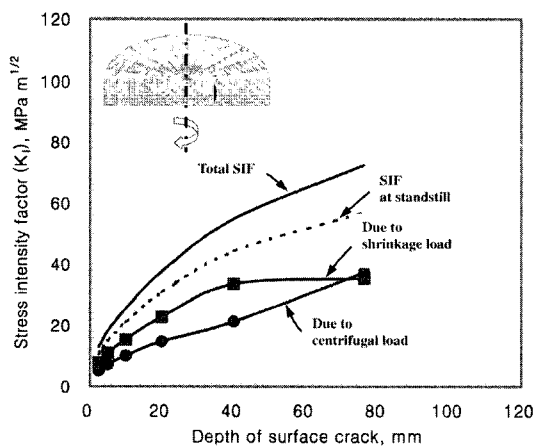

Fig. 7 Stress intensity factors calculated for the semi-elliptical surface cracks $(2c/a=5)$ located inside the center bore of the flywheel disc and contributed by the centrifugal load and shrinkage load acting on the flywheel at the normal operation speed
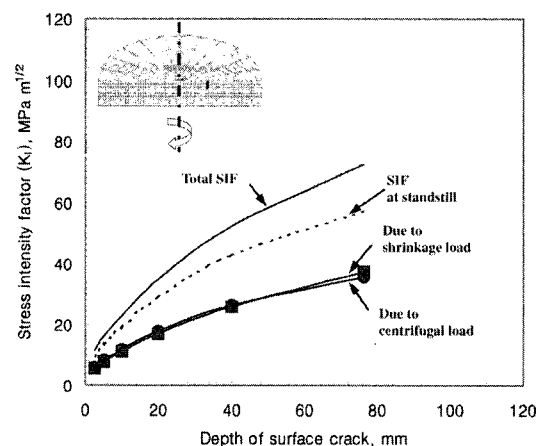

Fig. 8 Stress intensity factors calculated for the quarter-elliptical surface cracks $(2c/a=5)$ located inside the center bore of the flywheel disc and contributed by the centrifugal load and shrinkage load acting on the flywheel at the normal operation speed

up to the normal operation speed the shrinkage stress contributes major part of the crack driving force while the centrifugal stress does when exceeding the normal speed. The crack driving force caused by the shrinkage stress disappears at the joint-release speed.

Stress intensity factor ranges (ΔK) for different sizes of semi-elliptical or quarter-elliptical surface cracks are calculated between the stand-
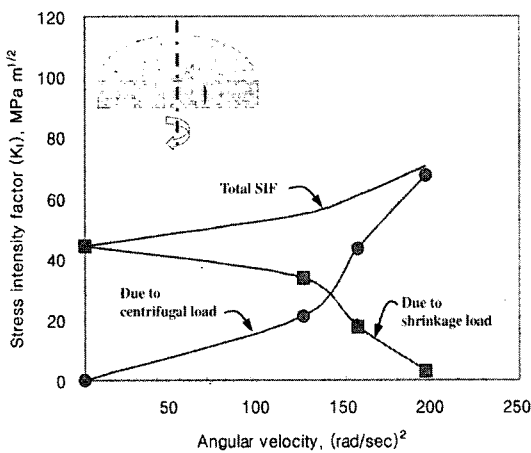

Fig. 9   Stress intensity factors calculated for the semi-elliptical surface crack $(2c/a=5, a=40$ mm) located inside the center bore of the flywheel disc at the standstill and rotating speeds of 1200, 1500, and 1875 rpm
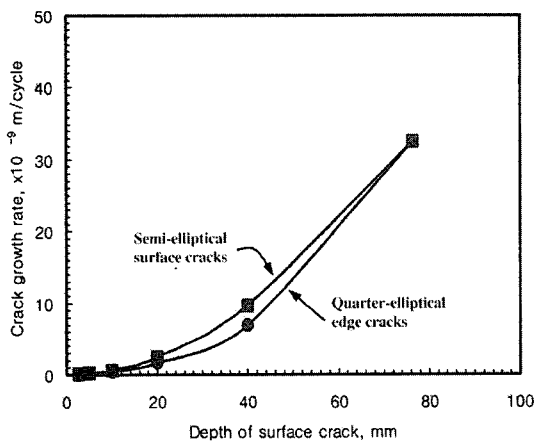

Fig. 10   Fatigue crack growth rates calculated for the semi-elliptical surface cracks and quarter-elliptical edge cracks $(2c/a=5)$ located inside the center bore of the flywheel disc

still and normal operation conditions of the flywheel assembly. Then fatigue crack growth rates (CGRs) are determined using the relationship in Eq. (4) and the results are presented in Fig. 10. The as-calculated CGRs for surface and edge cracks with the same depth of $a=40$ mm are 9.73×10^{-9} m/cycle and 6.97×10^{-9} m/cycle, respectively, which correspond to ΔK values of 10.53 MPa m$^{1/2}$ and 9.45 MPa m$^{1/2}$. These values appear relatively low compared to other type of flywheels with key (Riccardella et al., 1974). For the full-thickness crack at a depth of $a=76.25$ mm, the ΔK value between the standstill and the normal operation is found to be 15.61 MPa m$^{1/2}$. For the same depth, ΔK values for the semi-elliptical cracks are slightly higher than the ones for the edge cracks. For a conservative estimation of the fatigue growth during the plant lifetime, a CGR of 3.25×10^{-8} m/cycle in the radial direction is used considering the full-thickness crack (corresponding to $\Delta K=(15.61$ MPa m$^{1/2})$. Applying the total 4000 cycles into Eq. (4) the RCP starts and shutdowns during the 40-year plant life, the total fatigue crack growth of 0.13 mm at the end of the plant life is resulted and is negligible even with such a large initial crack.

The non-ductile fracture evaluations for the flywheel are conducted in accordance with the rules of Appendix G of Section III of the ASME Code. A summary of the evaluations is shown in Table 2, with the applied stress intensity factors (K_I) for both the normal operation (50 deg.C) and faulted conditions (design overspeed) and the fracture toughness of material $(K_{IC}$ as the minimum required). The value of applied K_I is the sum of stress intensity factors contributed by the primary and secondary stresses. A factor of 2 is applied to the K_I value due to the primary stress at normal operation condition. It is noted

Table 2   Summary of flywheel non-ductile fracture analyses

Service conditions	Applied K_I (MPa m$^{1/2}$)	Material K_{IC} (minimum)
Normal	109.77	165 MPa m$^{1/2}$
Faulted	81.37	(150 ksi in$^{1/2}$)

that the applied K_I in the normal service condition is higher and more limiting for the case of interference-fit flywheel analyzed.

In view of the excessive deformation, changes in the bore radius and the outer radius of the flywheel disc at the design overspeed are concerned. For the given values of initial interference for the flywheel, the radial deformation at the interface of the intermediate bushing to flywheel disc is calculated as 0.35 mm and that at the outer radius point of the flywheel disc as 0.28 mm. The flywheel deformation is proportional to the angular velocity (ω^2) and this represents an increase of 56% over the normal operating condition. The calculated deformations for the flywheel are negligible, and this would not result in any adverse conditions, e.g., vibration stresses leading to crack propagation.

4. Conclusions

The following concluding remarks can be drawn from the results of this study, while the FEM and FEAM models developed for stress analyses and fracture mechanics evaluations for the interference-fit flywheel need somehow verifications :

(1) The fatigue crack growth rates in the order of 10^{-8} m/cycle as determined for the smaller surface cracks in the flywheel, with a depth of 20 mm or less, are found to be negligible for the 40-year (even upto the 60-year) design life.

(2) The material resistance in terms of K_{IC} and RT_{NDT} to non-ductile fracture in the normal operating condition is the governing factor to ensure the structural integrity of the RCP flywheel with larger cracks.

(3) When applying design rules of interference-fit flywheels analogous to those of pressure vessels, lower stress acceptance criteria should be established since no plastic deformation in the flywheel is allowed.

References

ASME Boiler and Pressure Vessel Code, 2001,

Section II — Material Specification, American Society of Mechanical Engineers.

ASME Boiler and Pressure Vessel Code, 2001, Section III — Nuclear Power Plant Components, American Society of Mechanical Engineers.

ASME Boiler and Pressure Vessel Code, 2001, Section XI — Rules for Inspection and Testing of Components of Light-Water Cooled Plants, American Society of Mechanical Engineers.

Bae, D. H., Kwon, S. D, Song, S. J. and Lee, Y. Z., 2002, "Nondestructive Evaluation of the Characteristics of Degraded Materials Using Backward Radiated Ultrasound," *KSME International Journal*, Vol. 16, pp. 1084~1092.

Hibbit, Karlsson & Sorensen, Inc., 1998, ABAQUS/Standard User's Manual, Version 5.8, Providence, RI.

Kamaya, M. and Nishioka, T., 2004, "Evaluation of Stress Intensity Factors by Finite Element Alternating Method," PVP-Vol. 481, RPV Integrity and Fracture Mechanics, ASME, pp. 113~120.

Nikishkov, G. P., Park, J. H. and Atluri, S. N., 2001, "SGBEM-FEM Alternating Method for Analyzing 3D Non-planar Cracks and Their Growth in Structural Components," *Computer Modeling in Engineering and Science*, Vol. 2, pp. 401~422.

Park, J. H., Park, S. Y., Kim, M. W., Park, J. S. and Jin, T. E., 2004, "Development of a Code for 2D Elasto-Plastic Fracture Mechanics Analyses Using the Finite Element Alternating Method," *Key Engineering Materials*, Vols. 270-273, pp. 1159~1164.

Riccardella, P. C. and Bamford, W. H., 1974, "Reactor Coolant Pump Flywheel Overspeed Evaluation," *Journal of Pressure Vessel Technology*.

Song, J. I., Kim, S. and Shim, Y. L., 2002, "Residual Stress and Fracture Analysis of Thick Plate for Partial Penetration Multi-Pass Weldment," *KSME International Journal*, Vol. 16, pp. 1033~1039.

USNRC Regulatory Guide 1.14, 1975, "Reactor Coolant Pump Flywheel Integrity," Rev.1.

USNRC Information Notice No. 84-92, 1984, "Cracking of Flywheels on Cummins Fire Pump Diesel Engines".